

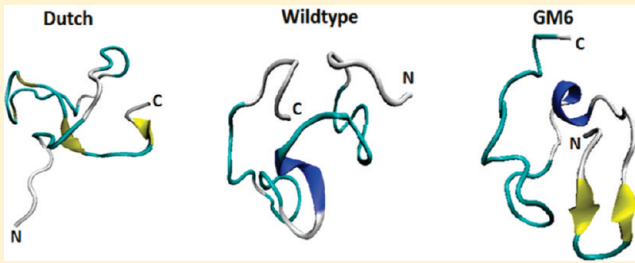
# Characterizing the Structural Behavior of Selected A $\beta$ -42 Monomers with Different Solubilities

Camilo Velez-Vega and Fernando A. Escobedo\*

School of Chemical and Biomolecular Engineering, Cornell University, Ithaca, New York 14853, United States

 Supporting Information

**ABSTRACT:** The conformational behavior of the wild-type amyloid  $\beta$ -42 ( $A\beta$ -42) monomer and two of its mutants was explored via all-atom replica exchange molecular dynamics simulations in explicit solvent, to identify structural features that may promote or deter early-stage oligomerization. The markers used for this purpose indicate that while the three peptides are relatively flexible they have distinct preferential structures and degree of rigidity. In particular, we found that one mutant that remains in the monomeric state in experiments displays a characteristic N-terminal structure that significantly enhances its rigidity. This finding is consistent with various studies that have detected a reduction in oligomerization frequency and  $A\beta$ -related toxicity upon sequence-specific antibody or ligand binding to the N-terminal tail of wild-type monomers, likely leading to the stabilization of this region. In general, our results highlight a potential role of the N-terminal segment on  $A\beta$  oligomerization and give insights into specific interactions that may be responsible for promoting the pronounced structural changes observed upon introducing point mutations on the wild-type  $A\beta$ -42 peptide.



## INTRODUCTION

Alzheimer's disease (AD) is a major health issue worldwide. In the U.S. alone, more than 5 million people are affected, a number that is projected to triple by the year 2030. AD is a neurodegenerative condition, pathologically characterized by the accumulation of extracellular plaques of amyloid  $\beta$ -protein ( $A\beta$ ) and the intracellular formation of neurofibrillary tangles of tau  $\beta$ -protein. The  $A\beta$  cascade mechanism is currently the leading hypothesis for the onset and progression of AD, a process believed to be triggered by an age-related increase in the production of the  $A\beta$ -42 protein (amyloid peptides of length 42 amino acids) relative to the more common and less neurotoxic  $A\beta$ -40 peptide.<sup>1</sup> An increase in the  $A\beta$ -42/ $A\beta$ -40 ratio promotes aggregation of improperly folded  $A\beta$  monomers, leading to the formation of oligomers and amyloid plaques/fibrils and ultimately to neuron cell damage. In the past decade, an increasing number of studies have reported that oligomers, and not fibrils, may be the primary neurotoxic agents (for a review, see ref 1). As a result, much of the research has thereafter shifted from the study of fibril formation pathways toward the elucidation of monomer/oligomer structural characteristics and their aggregation mechanisms. Low molecular weight oligomers ranging from dimeric to octameric aggregates are currently believed to be the smallest soluble  $A\beta$  species responsible for decreased synapse density, a marker that best correlates with the extent of dementia in AD.<sup>2–6</sup> Further examination of the  $A\beta$ -40 and  $A\beta$ -42 aggregates (which appear to follow different oligomerization pathways<sup>3,4</sup>) has led to a common belief that the structure of the oligomers varies with size and monomer type.<sup>4,5,7,8</sup> Unfortunately, experimental

studies aimed at the detailed characterization of oligomeric and monomeric structures (e.g., crystallization) at physiological conditions have been greatly hindered by the  $A\beta$ 's high aggregation rates, as well as their sensitivity to specific physicochemical conditions. Nevertheless, distinctive features of the monomers in water have been elucidated using NMR techniques for the  $A\beta$ -40<sup>9</sup> and  $A\beta$ -42<sup>10</sup> peptides. Other studies have focused on structural resolution of less amyloidogenic  $A\beta$  fragments<sup>9,11–14</sup> or within environments that discourage aggregation.<sup>13–17</sup>

Further insights into the  $A\beta$  monomer/oligomer structures and their aggregation mechanism have been derived from diverse computational approaches. Numerous groups have studied specific segments believed to be central for oligomerization or folding nucleation (using implicit<sup>18–26</sup> or explicit<sup>27–38</sup> solvent), whereas others have modeled the complete  $A\beta$  wild-type/mutant structures (using implicit<sup>39–44</sup> or explicit<sup>45–49</sup> solvent). Notably, dissimilar results for analogous systems are found in many of these studies; such inconsistencies can be mainly attributed to the specific sequence and length of the modeled segments, as well as to the effect of the force field and solvation model on the dynamics of this flexible peptide. While most of these studies may correctly describe some monomer/oligomer features, like total  $\beta$ -sheet/helical content, that have been estimated from experimental analyses (though these have also reported inconsistent findings), full validation of an appropriate

**Received:** September 10, 2010

**Revised:** March 25, 2011

in silico model for  $\text{A}\beta$ s and their aggregates at physiological conditions would entail comparison with yet-known experimental structures. Despite the latter, researchers have been able to improve the reliability of their simulations by matching their models with available experimental data (e.g., NMR restraints) or by comparison of structures from different force fields and solvation models. Of particular interest are the studies by Sgourakis et al.<sup>45,46</sup> and Krone et al.,<sup>27</sup> who independently identified the OPLS-AA<sup>50</sup>/TIP3 solvent<sup>51</sup> model as one that appropriately represents the 21–30 fragment<sup>27</sup> and the full  $\text{A}\beta$  monomers.<sup>46</sup> These results are consistent with our own preliminary search for a satisfactory  $\text{A}\beta$  model, in which we explored different force fields with implicit and explicit solvent models. Moreover, we found that the study of the complete monomer in explicit solvent is important for the detection of structural features such as secondary structure content at the Central Hydrophobic Core<sup>10</sup>—residues (RES) 17–21—and specific electrostatic interactions like those observed in experiments between E22 or D23 and K28.<sup>52</sup>

In the present study, we report our findings on the changes in structural behavior of  $\text{A}\beta$ -42 upon mutation, by simulating the complete wild-type (WT)  $\text{A}\beta$ -42 and two mutants of this peptide. We carried out explicit solvent simulations using a novel adaptation of replica exchange molecular dynamics (REM),<sup>53</sup> called All Pairs Exchange (APE),<sup>54</sup> that significantly enhances the efficiency of REM sampling.

With the intent of identifying key differences in the monomers that may promote dissimilar dimerization mechanisms (as a first step toward higher-order oligomerization), the two  $\text{A}\beta$ -42 mutants of the WT to be simulated were carefully selected based on the following: (1) For the first mutant, namely, the soluble variant, there should be experimental evidence of a markedly lower aggregation rate with respect to the one observed in experiments for WT  $\text{A}\beta$ -42. (2) For the second mutant (i.e., the insoluble variant), it was also required to have experimental data for a markedly higher aggregation rate compared to the one reported for WT  $\text{A}\beta$ -42. (3) Both the soluble and the insoluble variants should have the fewest possible number of mutations since each additional residue that is mutated from the WT sequence implies a nonlinear increase in the number of new inter-residue interactions, making it harder to correlate these interactions with structural changes. Thus, by keeping the number of mutations as low as possible, we reduce the complexity of identifying these differences within the monomers. A literature search for mutants that met these restrictions led to the selection of GM6 as a suitable choice for the soluble variant and the Dutch mutant as the insoluble variant. Specifically, we chose GM6 (F19→S19, L34→P34) because it has consistently displayed virtually no aggregation in several in vitro studies<sup>55–57</sup> using different “folding quality” assays. Moreover, to our knowledge, a structural analysis of the complete GM6 monomer has not yet been performed, making its study a novel contribution that can provide valuable insights into interactions that may modulate the solubility of  $\text{A}\beta$ -42 at the monomer level. Similarly, we selected the Dutch (E22→Q22)  $\text{A}\beta$ -42 as the insoluble variant, given that it has shown a considerably faster in vitro aggregation rate than that of WT  $\text{A}\beta$ -42.<sup>58</sup> Most of the studies on the Dutch type have focused on the 40-residue monomer, due to its apparent role in hereditary cerebral hemorrhage with amyloidosis Dutch-type (HCHWA-D).<sup>59–62</sup> However, we targeted our analysis on the 42 length monomer, given that both its in vitro neurotoxicity and aggregation rate are appreciably higher than

those of the WT  $\text{A}\beta$ -42 and Dutch  $\text{A}\beta$ -40 variant;<sup>58,63</sup> in addition, this selection allows the study of relevant discrepancies between electrostatic interactions involving residues 41 and 42. (Unless otherwise noted, for the remainder of this document, it is assumed that all mutant types are 42 amino acids long.) Additional motivation for the study of the Dutch  $\text{A}\beta$ -42 mutant comes from the fact that, to our knowledge, only segments of this peptide have been studied (e.g., RES 15–28,<sup>28</sup> RES 10–35,<sup>64</sup> RES 21–30<sup>65</sup>); i.e., no detailed structural modeling of the complete monomer has yet been reported.

In the following section, we provide a brief description of the model setup and simulation approach. Our results for the  $\text{A}\beta$ -42 mutagenesis analysis are then presented, followed by a discussion of our findings and some concluding remarks.

## ■ EXPERIMENTAL METHODS

**Monomer Simulations.** The configuration space of the Dutch, WT, and GM6  $\text{A}\beta$ -42 monomers was explored using the OPLS-AA/TIP3P water model, via REM/APE simulations in the GROMACS<sup>66</sup> molecular simulation package. The APE method considerably increases the probability of generating an exchange between pairs of replicas while meeting the detailed balance condition. For various systems previously studied by our group, REM/APE reduced at least by a factor of 2 the simulation time required for configurational sampling compared to conventional REM.<sup>67</sup>

The systems were prepared as follows. The structure of  $\text{A}\beta$ -42 in an apolar solvent (PDB code: 1IYT)<sup>19</sup> was mutated for the Dutch and GM6 variants and energy minimized using the Steepest Descent algorithm. After peptide solvation and neutralization of the system, we heated the resulting structure to 700 K and carried out a 10 ns MD simulation at constant temperature using a Nose-Hoover<sup>68,69</sup> thermostat (employed for all of our simulations), from which a random coil structure was obtained. (The solvated random coil structures were used for exploratory studies aimed at optimizing the simulation time required for this analysis.) The time step for all our simulations was 2 fs, as allowed by the use of the LINCS<sup>70</sup> algorithm for constraining bond lengths. The coiled conformation was then collapsed by means of a 5 ns vacuum simulation at the same 700 K that allowed resolvation of the peptides in 3393 (Dutch = 3371, GM6 = 3401) molecules of TIP3P water. This was followed by a short MD run at 300 K for equilibration of the water box, in which the position of the peptide was restrained. A 1 ns MD simulation at  $P = 1$  atm and  $T = 300$  K was then carried out for equilibration of the whole water–protein system. The WT, Dutch, and GM6 structures thus obtained were used as starting conformations for our REM/APE simulations. We note that our procedure for generating initial structures, analogous to the one used by Sgourakis et al.,<sup>46</sup> considerably facilitates the simulation of the complete  $\text{A}\beta$  structure in explicit solvent by solvating a rather collapsed peptide instead of an otherwise extended conformation, which would require a significantly higher number of water molecules for its solvation. It could be argued that sampling may be hampered when a collapsed coil structure is used as the initial conformation. However, a detailed validation of this model using NMR  $^3\text{J}$ -coupling constants<sup>46</sup> and the use of REM/APE to promote rapid conformational sampling makes this approach very suitable for modeling the dynamics of  $\text{A}\beta$ -42.

REM/APE simulations were carried out for the three cases in the 250–600 K range. Swaps were attempted every 1 ps, and an

exchange probability close to 20% was targeted, requiring 32 replicas that were exponentially distributed along the temperature range. The GM6, WT, and Dutch systems were, respectively, run for 45, 55, and 85 ns/replica (corresponding to a total of 1.44, 1.76, and 2.72  $\mu$ s), saving configurations every 1 ps. For each case, the data acquired for the replicas at 296 K were used for the analysis presented in the Results section. We note that, in all cases, the statistics obtained for three other replicas at 288, 305, and 313 K are consistent with the ones reported at 296 K. All of our REM/APE simulations were run in the NIC of Corning Inc.

**Analysis Tools.** Unless otherwise noted, our analyses are performed on the ensemble gathered at room temperature (i.e., 296 and 298 K for our REM/APE and MD simulations, respectively). The Single Linkage and Jarvis Patrick clustering methods available through the g\_cluster tool in GROMACS were employed to group the 10 000 conformations analyzed for each monomer. Both methods identified analogous dominant clusters for all cases; however, the more stringent Jarvis Patrick algorithm consistently produced a higher number of clusters. Given that for the three monomers studied a few clusters are able to group the majority of the ensemble structures, the results presented in the *cluster analysis* section correspond to those obtained via the Single Linkage method. The central (i.e., typical) structures for each cluster were obtained directly from these calculations.<sup>66</sup> Contact maps were generated using the g\_mdmat tool in GROMACS, which identifies the minimum distance between residues by calculating the smallest distance between any pair of atoms belonging to distinct residues. A truncation distance of either 1.0 or 1.5 nm was employed for the contact map calculations.  $S^2$  order parameters for each main chain N–H bond were calculated by averaging the converged portion of the corresponding rotational autocorrelation function, obtained by means of the g\_rotafc tool in GROMACS. Secondary structure analyses were carried out using the DSSP<sup>71</sup> program, which interfaces with GROMACS through the do\_dssp tool. For analysis of hydrogen bonds we used a cutoff distance of 3.5 Å.

Schematic representations of peptides were achieved via the VMD<sup>72</sup> program. All other calculations were performed using tools available in GROMACS.

## RESULTS

Several analyses were performed to identify differences between the monomers' conformational ensembles; these disparities may help clarify the dissimilar dimerization/oligomerization rates and mechanisms observed in experiments for these peptides. The results presented in this section were extracted from representative time periods at 296 K for each case: 35–45 ns, 35–55 ns, and 60–85 ns periods for the GM6, WT, and Dutch monomers, respectively. Details on the selection of the representative time periods are given in the Supporting Information.

**Structural Stability.** We initially performed an  $S^2$  order parameter analysis to assess the relative rigidity of the complete  $\text{A}\beta$ -42 monomers and their key regions, namely, the Central Hydrophobic Core (CHC, RES 17–21) and the 10-residue N and C terminal segments. Figure 1 shows average values of the regions analyzed, for the ensembles at room temperature (296 K) during the representative periods. When all residues are considered, a relative decrease in the rigidity of the peptides is observed, with  $S^2_{\text{GM6}} > S^2_{\text{WT}} > S^2_{\text{Dutch}}$ . However, the Dutch and WT monomers still have similar  $S^2$  values compared to GM6.

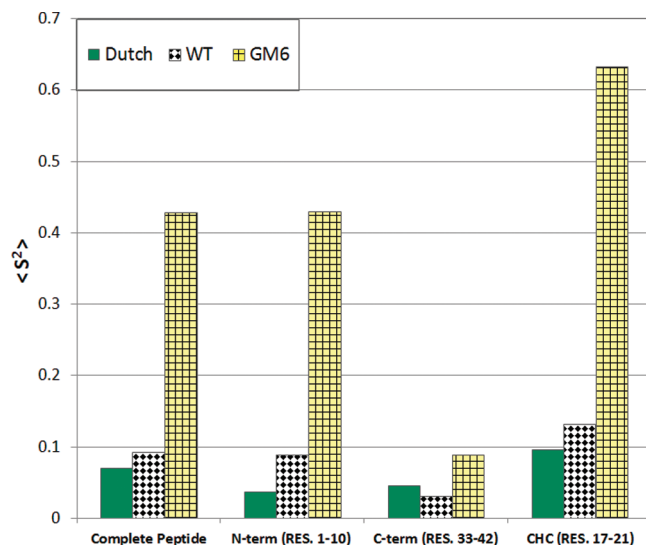


**Figure 1.**  $S^2$  order parameters for the monomers studied. Average values are shown for the complete protein, N-terminal, C-terminal, and CHC regions.

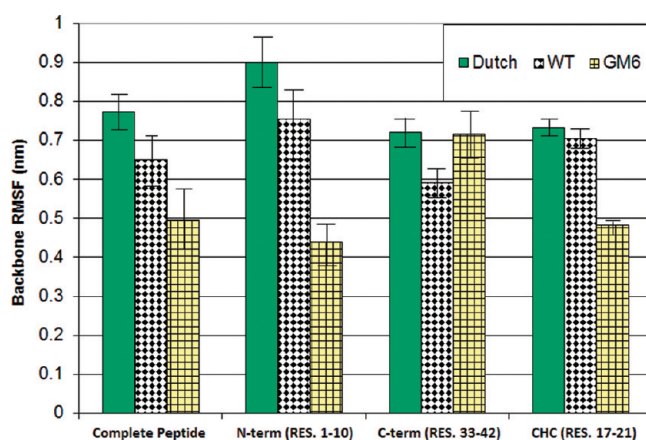


**Figure 2.** Average backbone RMSF for the monomers studied. Values for the complete protein, N-terminal, C-terminal, and CHC regions are shown. The bars represent the standard deviation for each case.

Upon analysis of the key  $\text{A}\beta$  regions, we found that the difference in relative stability of the three peptides is most evident among their N-terminal segments (RES 1–10, Figure 1). Interestingly, the relative decrease in the N-terminal stability of the GM6, WT, and Dutch variants is consistent with the experimentally observed decline in their relative aggregation rate. This result does not imply a direct relationship between the N-terminal rigidity of the  $\text{A}\beta$ -42 monomers and their complex aggregation mechanism but points to a distinguishing structural feature of these peptides that may be relevant to oligomerization dynamics. Conversely, for the C-terminal region, the WT shows a lower rigidity than the remaining two peptides, both of which still display low  $S^2$  values. We note that some experimental<sup>73</sup> and computational<sup>46</sup> studies have found the C-terminal of WT  $\text{A}\beta$ -42 to be less flexible than that of the more soluble WT  $\text{A}\beta$ -40, leading to the proposal that an increasingly stable C-terminal is more likely to seed aggregation. In contrast, our results suggest that both a more soluble (GM6) and a less soluble (Dutch)  $\text{A}\beta$ -42 variant can have a

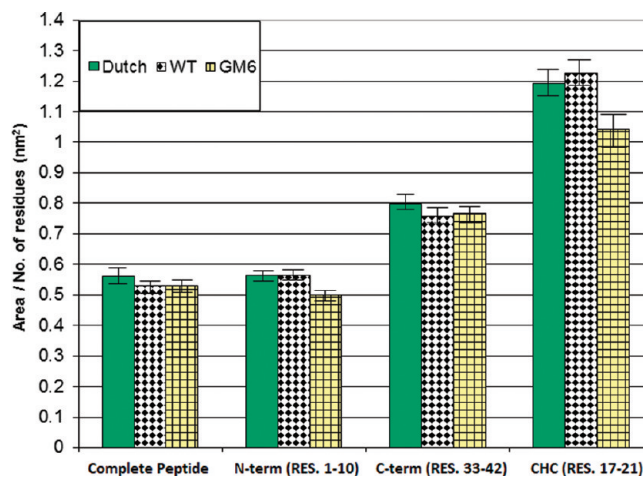


**Figure 3.** Hydrophobic Solvent Accessible Surface Area of the monomers studied, normalized by the number of residues in each segment. Values for the complete protein, N-terminal, C-terminal, and CHC regions are shown. The bars represent the standard deviation for each case.

C-terminal that is more flexible than that of WT A $\beta$ -42. Figure 1 also shows clear flexibility differences of the CHC among peptides, with the GM6 displaying significantly higher stability, likely due to the residue-specific interactions discussed later in this work. The CHC region has been proposed as a site for aggregation initiation, due to potential destabilization of the monomer's secondary structure.<sup>21</sup> While the GM6 result is consistent with this view, the small difference between the S<sup>2</sup> order parameters in the Dutch and WT CHC regions would indicate comparable flexibilities. We note that the absence of experimental S<sup>2</sup> data for these 42-long monomers prevents us from performing any quantitative validation; to our knowledge, only values for shorter, more soluble A $\beta$  peptides have been reported to date.<sup>9</sup>

To complement the previous findings, we also evaluated the backbone Root Mean Square Fluctuation (RMSF<sub>back</sub>, understood as the standard deviation of the backbone's atomic positions with respect to their mean values). Figure 2 shows the average RMSF<sub>back</sub> (nm) values and corresponding standard deviation (SD) of the key A $\beta$ -42 regions. The results are in good agreement with those from the S<sup>2</sup> parameter analysis. We observe a statistically significant difference in the flexibility (i.e.,  $\overline{\text{RMSF}}_{\text{back}}^{\text{Dutch}} > \overline{\text{RMSF}}_{\text{back}}^{\text{WT}} > \overline{\text{RMSF}}_{\text{back}}^{\text{GM6}}$ ) for both the complete peptides and their N-terminal regions. Moreover, the C-terminal of the WT again appears to be more rigid than those of the Dutch and GM6 mutants, for which no statistically significant difference is observed. Similarly, the  $\overline{\text{RMSF}}_{\text{back}}$  for the CHC confirms that the difference in this region's rigidity between the Dutch and WT monomers is not statistically significant. The latter finding undermines the idea that the monomer's CHC destabilization is a driving force for oligomerization<sup>21</sup> but still allows for a cooperative interplay between the CHC and other A $\beta$ -42 regions (e.g., interactions with N-terminal residues) upon aggregation, leading to the experimentally observed solubility differences.

The Hydrophobic Solvent Accessible Surface Area (SASA<sub>Hphi</sub>) of the system was also monitored for all the monomers. Figure 3 shows the ensembles' SASA<sub>Hphi</sub> and corresponding SD for the complete peptide and the key A $\beta$  regions, normalized by the number of residues analyzed for each case. Notably, the only

statistically significant differences in SASA<sub>Hphi</sub> among the monomers are those observed between the N-terminal and CHC segments of GM6 and the corresponding regions of the WT and Dutch variants. The visibly lower SASA<sub>Hphi</sub> value of GM6's CHC region is a direct consequence of the F19S (nonpolar  $\rightarrow$  polar) mutation in this short region. This is not the case for RES 1–10, given that this segment has the same sequence for all mutants. A reduced SASA<sub>Hphi</sub> in this N-terminal region of the GM6 mutant implies a lower energetic cost for solvation, in congruence with the higher solubility found experimentally for this mutant.<sup>55</sup> In contrast, comparable SASA<sub>Hphi</sub> values between the C-terminal regions of the Dutch, WT, and GM6 peptides suggest that the peptides would have a similar proclivity to minimize exposed hydrophobic regions by dimerization/oligomerization contacts at this segment. Of course, this finding does not rule out the hypothesis of C-terminal clustering as a driving force for A $\beta$  oligomerization,<sup>44</sup> given that our results for monomer models are unable to identify potentially favorable energetic interactions between C-terminals upon oligomerization.

In an effort to further recognize specific hydrophobic interactions that can modulate the solubility of the monomers, we searched for contacts between the  $\beta$ -carbons of hydrophobic residue side chains (1 nm threshold). The contact maps for the three peptides are similar (Figure 4) and display five hydrophobic pockets, corresponding to: (1) index 1–2 (WT and Dutch, RES. 2, 4) or index 1–3 (GM6, RES. 2, 4, and 12), (2) index 4–9 (WT and Dutch, RES. 17–21 and 24) or index 4–8 (GM6, RES. 17–18, 20–21, and 24), (3) index 10–12 or index 9–11 (all cases, RES. 30–32), (4) index 13–15 (WT and Dutch, RES. 34–36) or index 12–13 (GM6, RES. 35–36), and (5) index 16–19 or index 14–17 (all cases, RES. 39–42). Local hydrophobic associations 3 and 5 are analogous for all monomers, whereas 2 and 4 differ for GM6 (the pocket involves fewer residues) given that it lacks hydrophobic residues at positions 19 and 34. The most notable difference between GM6 and the insoluble mutants is then its nonlocal hydrophobic pocket 1. This interesting feature likely aids the stabilization of the GM6 monomer structure and, particularly, its N-terminal, by restraining the motion of residues therein.

In addition, the total energy of the solvated system ( $E$ ) was measured as a tentative marker of the monomers' relative "folding quality". Specifically, for systems of analogous size, given that the enacted point mutations introduce relatively small perturbations to the basal energy of the system, it is expected that the more "native-like" variants readily sample lower-energy regions. In order of decreasing values, lower-energy regions are sampled by the Dutch ( $E_{\text{average}} = -108\,817$  kJ/mol,  $\sigma = 672$  kJ/mol), WT ( $E_{\text{average}} = -114\,146$  kJ/mol,  $\sigma = 528$  kJ/mol), and GM6 ( $E_{\text{average}} = -118\,365$  kJ/mol,  $\sigma = 443$  kJ/mol) variants. Moreover, we calculated the energy change  $\Delta E = E_{\text{average}}(600\text{ K}) - E_{\text{average}}(296\text{ K})$  for each monomer as an approximate indicator of the relative energy difference between the random coil states at our highest simulation temperature and the structured states found at 296 K. The increasing values of  $\Delta E_{\text{Dutch}} = 76\,034$  kJ/mol,  $\Delta E_{\text{WT}} = 79\,532$  kJ/mol, and  $\Delta E_{\text{GM6}} = 82\,478$  kJ/mol suggest that more native-like mutants have a stronger energetic driving force leading to a deeper energy minimum upon folding. The latter analyses suggest that the Dutch, WT, and GM6 monomers have increasingly enhanced "folding quality", a behavior that is consistent with the commonly accepted protein misfolding and aggregation hypothesis.<sup>74</sup> More accurate methods that can factor out completely the effect of the mutations (e.g., by comparing only

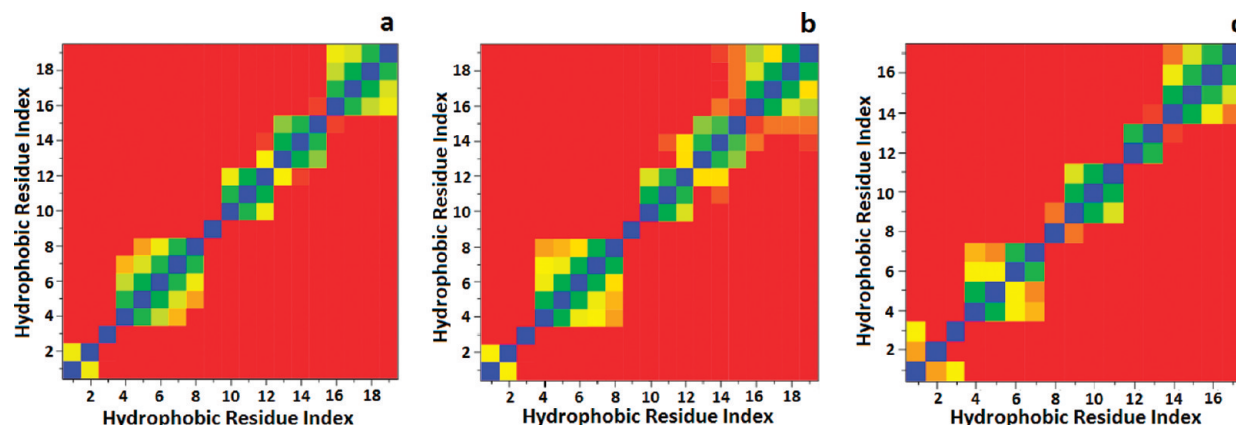


**Figure 4.** Contact maps for the  $\beta$ -carbons of the hydrophobic residue side chains, for the Dutch (a), WT (b), and GM6 (c) monomers. The plots are symmetric across the diagonal, and their  $x$  and  $y$  scales correspond to an index that goes from 1 to 17 (GM6) or 1 to 19 (WT and Dutch), with ticks representing the residues with hydrophobic side chains as they occur along the N–C direction of each sequence. The color scale ranges from 0 nm (blue) to 1.0 nm (red).

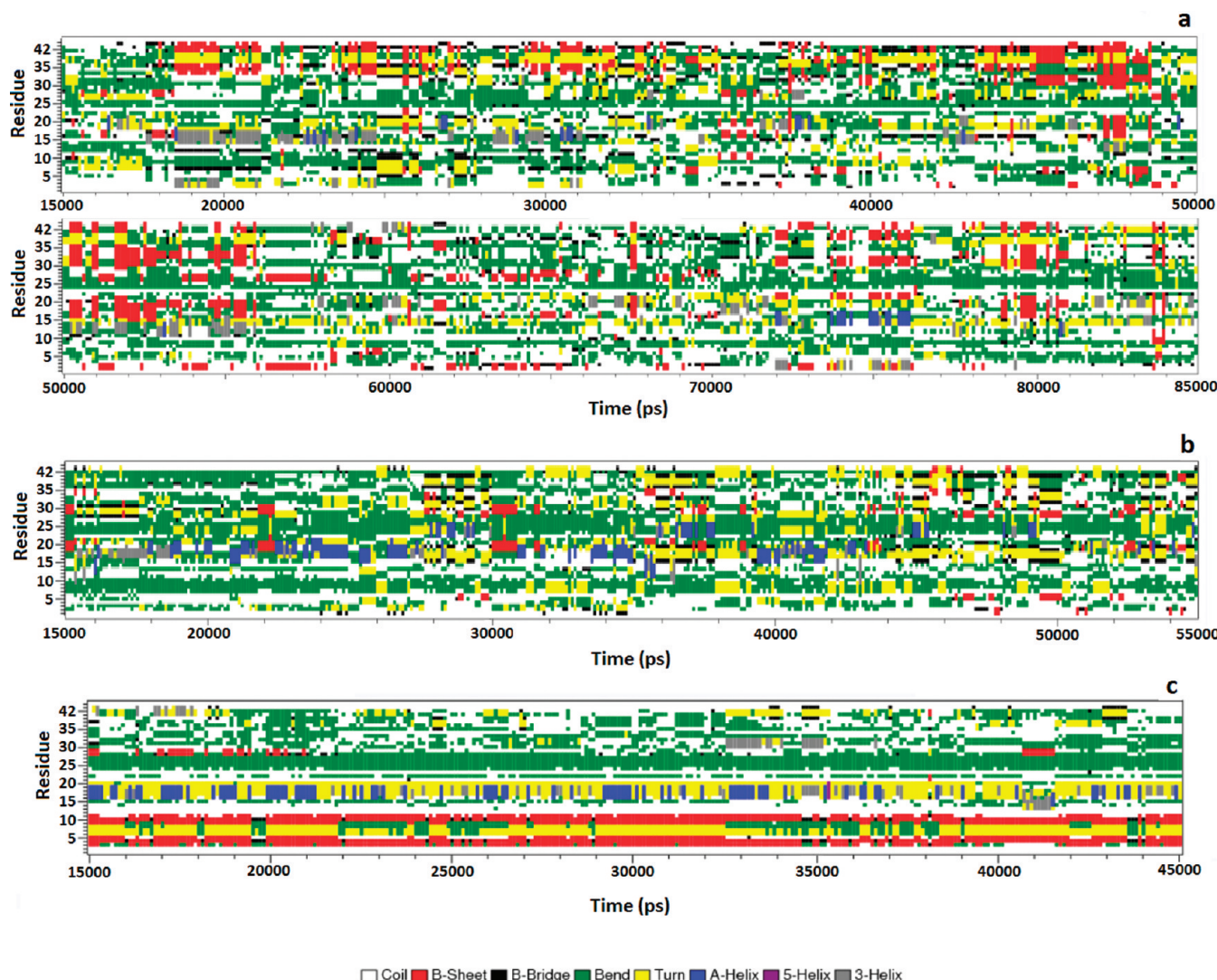


**Figure 5.** Secondary structure content of the monomers studied at 296 K. The plots correspond to the 15–85 ns, 15–55 ns, and 15–45 ns periods of the Dutch (a), WT (b), and GM6 (c) variants, respectively. For clarity purposes, only the structures saved every 100 ps are presented in the plots. The color code is included below plot c.

the interaction energies of the common residues, including those of residues with the water molecules) are currently being explored.

Lastly, we note that the number of *distinct* H-bonds found in the GM6 ensemble, 135 different pairs, is in clear contrast with that of the Dutch (324 pairs) and WT (276 pairs) structure sets. The reduced number of highly preserved H-bonds observed in the GM6 monomer, as opposed to the numerous short-lived H-bonds found in the other two variants, is consistent with its increased relative rigidity.

**Distinctive Structural Features.** We evaluated the peptides' representative conformation ensembles for the incidence of conserved structural motifs. Two complementary approaches, namely, a Secondary Structure Content (SSC) analysis and a clustering procedure, were used for this purpose. From the SSC analysis, we obtained the average SSC as well as secondary structure plots as a function of time and residue number for the Dutch (Figure 5a, 15–85 ns), WT (Figure 5b, 15–55 ns), and GM6 (Figure 5c, 15–45 ns) peptides. On the other hand, the clustering analysis performed on the representative ensembles led to 18 (Dutch), 11 (WT), and 10 (GM6) clusters, using an rmsd cutoff of 3 Å. Figure 6 shows the cluster populations for all cases; the central structures of the main clusters, representing about 60% of each ensemble, are shown as insets in each plot. In addition, Figure 7 presents the contact maps of the major clusters for each monomer, to highlight their inter-residue interactions.

In general, all peptides are mostly unstructured, with the following average SSC for the representative ensembles: random coil –48% (Dutch), 41% (WT), 40% (GM6);  $\beta$ -bridge/ $\beta$ -turn/bend –42% (Dutch), 52% (WT), 46% (GM6); helical –3% (Dutch), 4% (WT), 4% (GM6);  $\beta$ -sheet –7% (Dutch), 3% (WT), 10% (GM6). These results agree qualitatively with experimental studies that have observed secondary structure content in the Dutch,<sup>58</sup> WT,<sup>13,15</sup> and GM6<sup>55</sup> monomers. Quantitative agreement is not sought, given the approximate nature of the available experimental assays and the high rate of aggregation of the WT and Dutch peptides that may promote conformational changes upon oligomerization in early stages of the experiments.

Despite the apparent similarity among the average SSCs of the three peptides, they sample conformations with different local arrangements. It is readily observed that the Dutch (Figure 5a) and WT (Figure 5b) peptides visit a wide variety of structural arrangements, interchanging between numerous short-lived structural motifs along the whole extension of the peptide. This behavior contrasts with the one found for GM6 (Figure 5c), which displays conserved motifs at specific regions of the peptide throughout the simulation period. Importantly, Figure 5c shows a remarkably stable  $\beta$ -sheet (94% of the 15–45 ns ensemble) spanning N-terminal RES. 3–11 (<sup>3</sup>EFRHDSGYE<sup>11</sup>). This is the most distinctive and predominant structural difference found between the soluble GM6 peptide and the Dutch and WT monomers. We also observed several less frequent structural motifs in all of the peptides' ensembles, which we further characterize in the remaining of this section.

Concerning the most insoluble—Dutch—mutant, all of the central structures of its dominant clusters (clusters 1, 2, 3, and 4, Figure 6a) display a C-terminal  $\beta$ -hairpin in the <sup>35</sup>MVGGVIA<sup>42</sup> region and  $\beta$ -bridges at RES. 27/28 and RES. 32/33, both of which are intermittently observed in the SSC plot (Figure 5a). Figure 5a also shows recurrent formation of secondary structures at the CHC region and evidence of small stable motifs in residues 2 and 3, likely due to a strong local interaction between them. Nonetheless, the contact maps of the major clusters (Figure 7a)

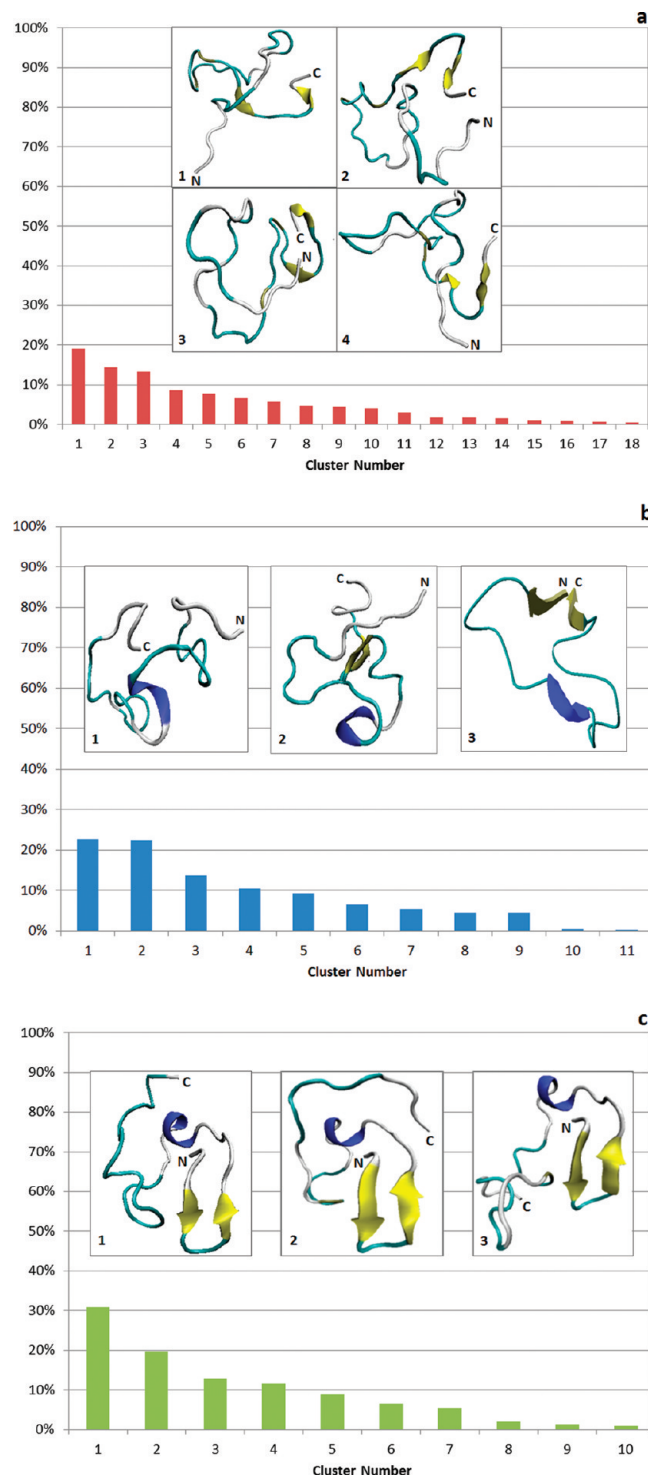


**Figure 6.** Relative population of the clusters identified for the Dutch (a), WT (b), and GM6 (c) ensembles at 296 K, for the representative periods. The central structures of each of the major clusters are shown as insets in the plots, colored by structure type (yellow =  $\beta$ -sheet, blue = helix, tan =  $\beta$ -bridge, cyan = turn + bend, and white = random coil). The number on the lower left corner of each central structure inset indicates the corresponding cluster.

display dissimilar inter-residue interactions, signaling the broad conformational sampling of this peptide. The contact maps of clusters 1, 3, and 4, accounting for 41% of the complete

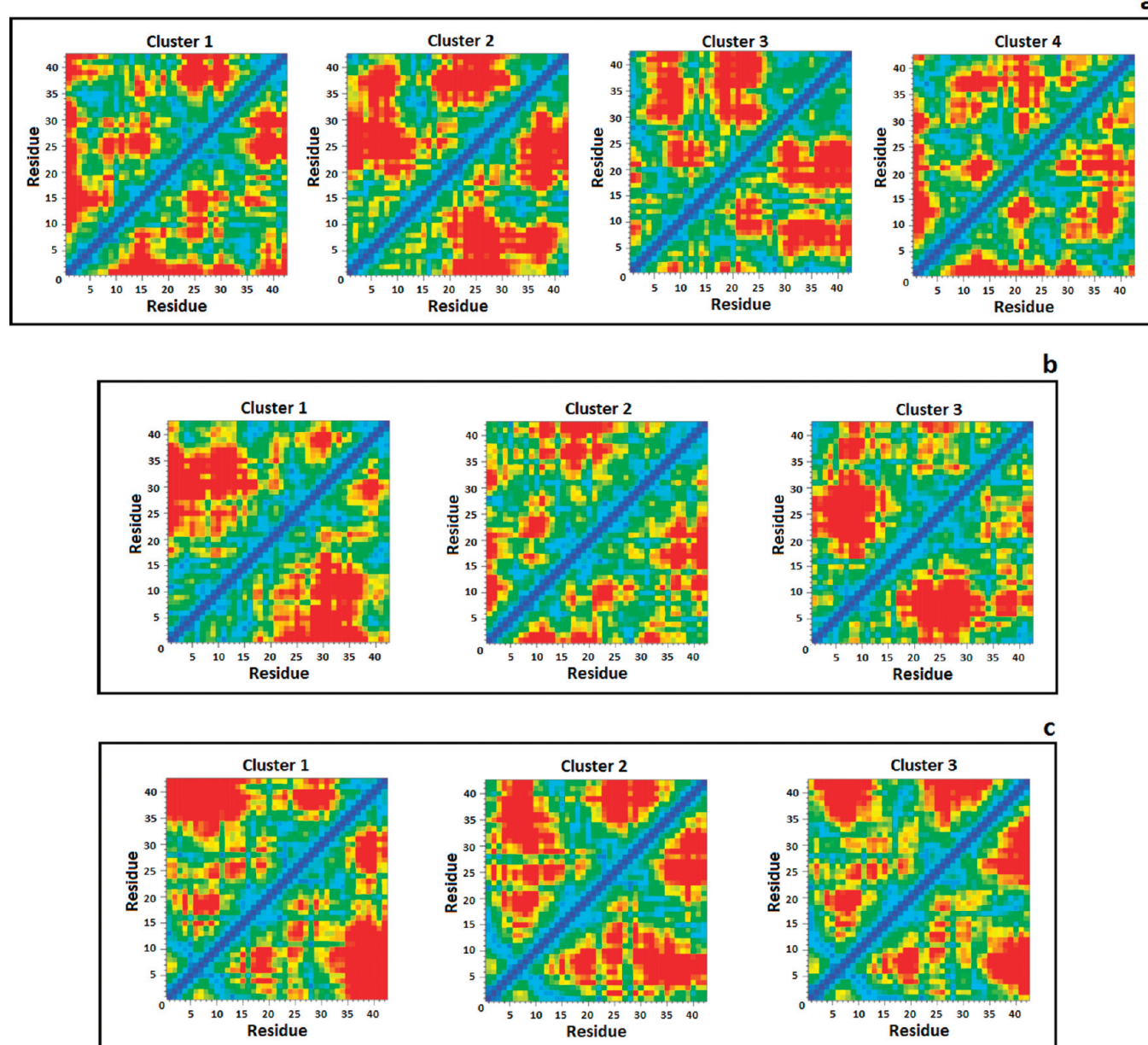


**Figure 7.** Contact maps for the major clusters of the Dutch (a), WT (b), and GM6 (c) monomers. The clusters presented account for 63% (Dutch, figure a), 59% (WT, figure b), and 63% (GM6, figure c) of the corresponding ensemble. All plots are symmetric across the diagonal, and their *x* and *y* scales go from 1 to 42, with ticks representing the residue numbers. The minimum distances between residues are represented by means of a color scale ranging from 0 nm (blue) to 1.5 nm (red).

ensemble, show that the N-terminal (RES. 1–10) is able to come in close contact with most regions of the peptide, evidencing a high N-terminal flexibility. Also, in the contact map for cluster 2 we find several contacts within the RES. 1–20 region, consistent with the convoluted but unstructured shape of the N-terminal observed for central structure 2.

Conversely, for the WT peptide we found the conserved helix at the CHC to be the most relevant trait of the major clusters' central structures (clusters 1, 2, and 3, Figure 6b). This agrees with the periodic occurrence of stable motifs at the CHC (Figure 5b). The WT monomer also displays a tendency to adopt a collapsed coil structure with extensive contacts within the RES. 20–30 segment, as evidenced by the contact maps of the

three major clusters (Figure 7b). Overall, the structural diversity derived from our WT ensemble is in good agreement with recent work by Sgourakis and co-workers.<sup>45,46</sup> Specifically, we remark that: (1) One of the larger WT clusters found in ref 45 is comparable to our dominant WT cluster, displaying a random coil structure with a short  $\alpha$ -helix either at the CHC (cluster 1, Figure 6b) or at RES. 21–24 (Figure 5f, ref 45). (2) Sgourakis et al. report the presence of a random coil WT conformation with a C-terminal  $\beta$ -hairpin between RES. 33–35 and RES. 40–42 (Figure 5b, ref 45) or between RES. 31–34 and RES. 39–42 (ref 46, 27% of their WT A $\beta$ -42 simulation ensemble); similarly, our clusters 2 and 9, corresponding to 26% of the ensemble, also show structures with C-terminal  $\beta$ -hairpin formation either

between RES. 33–35 and RES. 40–42 or between RES. 30–32 and RES. 34–36. (3) Specific interactions between the N and C terminal tails, such as conserved H-bonds between D1-A42, A2-V40, and E3-V40, were found in 36% of our WT ensemble. A distinctive instance of this arrangement is the central structure of cluster 3 (14% of the ensemble) which, in addition to showing an  $\alpha$ -helix at the CHC, exhibits a  $\beta$ -hairpin between RES. 1–3 and RES. 40–42. Interestingly, a comparable conformation was also observed in ref 45 (Figure 5a), displaying a  $\beta$ -hairpin between RES. 4–6 and RES. 38–40 and an  $\alpha$ -helix at RES. 8–12. Note that N–C tail interactions may be responsible for the increased stability of the WT  $A\beta$ -42 C-terminal region with respect to that of the Dutch (see Figures 1 and 2) and WT  $A\beta$ -40 variants. (4) Lastly, clusters 4 and 10, corresponding to 11% of the ensemble, display  $\beta$ -sheet interactions between RES. 20–22 and RES. 38–41 that closely resemble Figure 5c of ref 45.

Regarding the GM6 monomer, the central structures and contact maps of its major clusters (clusters 1, 2, and 3, Figures 6c and 7c) show a well-preserved N-terminal  $\beta$ -hairpin spanning the <sup>3</sup>EFRHDSGYE<sup>11</sup> segment, in good agreement with Figure 5c. Similarly to the WT and Dutch peptides, all GM6 central structures show helical content at the CHC, suggesting that this is a common feature among the  $A\beta$ -42 variants. The structures of the GM6 ensemble appear to be highly conserved for RES. 1–30 and differ only in the location of a more flexible C-terminal that lacks conserved stabilizing motifs. The contact maps of the major clusters are also consistent with the previous results; clusters 1 and 3 sample very similar configuration space (Figure 7c), whereas cluster 2 differs mainly in the emergence of interactions between RES. 36–42 and RES. 10–15 (with a corresponding decrease in the number of contacts in the intermediate region), changes promoted by the reduced distance between these segments. Additional features common to the major clusters are: (i) well-preserved contacts between either E22 or D23 and K28 and (ii) the extensive number of contacts between either E22 or K28 and RES. 1–20, which helps hold the peptide's N-terminal half together and contributes to its reduced flexibility. Moreover, we found that the ensemble structures periodically form a  $\beta$ -strand in RES. 27–29 that constantly interacts with the RES. 3–5  $\beta$ -strand region.

Overall, the study of the peptides' clusters gives useful insights into the tentative role of the stabilizing/destabilizing mutations. Specifically, we found that the F19S change in the GM6 variant causes the S19 side chain to stick out toward the solvent (unlike the WT F19 side chain which is buried inside the peptide), promoting a backbone rearrangement in the CHC which leads to the burial of the previously exposed E22 side chain and consequent formation of the strong stabilizing D1-E22 H-bond, along with other favorable hydrophobic and electrostatic interactions within the N-terminal. The L34P mutation in GM6 further boosts the prevalence of the latter interactions, by preventing the formation of the E22–L34 H-bond commonly observed in the WT. Likewise, for the Dutch variant, the E22Q mutation discourages the interaction between RES 22 and 34 (this contact stimulates close proximity between the N and C terminals of the WT), giving rise to stronger contacts in the intermediate region corresponding to RES. 15–30 (e.g., Q22–A21, Q22–V18). The relatively stable midregion of the Dutch monomer acts as a "hinge" for the more flexible N and C terminal segments, which display multiple but transitory local interactions.

## ■ DISCUSSION

Understanding the structural dynamics of the  $A\beta$  monomers is important to aid the design of selective therapeutics that can prevent their oligomerization and the resulting toxicity of these aggregates. However, despite numerous experimental and computational efforts, there is still not a clear picture of the key structural features of the monomers that may seed the oligomerization process. On the one hand, experimentally attaining high-resolution structures has been hindered by the  $A\beta$ 's fast aggregation rate; on the other hand, *in silico* modeling of the full monomer in explicit water still presents a significant computational challenge. Alternatively, given that the core structure of  $A\beta$  fibrils excludes the monomers' N-terminal,<sup>75</sup> many groups have focused on shorter/less amyloidogenic segments of the 11–40 (or 11–42)  $A\beta$  fragment. Remarkably, increasing evidence supporting a critical role of the N-terminal in  $A\beta$  aggregation has been reported by various experimental groups that have observed inhibition of oligomerization and fibril disaggregation upon N-terminal (mainly RES. 1–10) antibody or ligand binding.<sup>76,77</sup> Moreover, these studies concur that aggregation is not appreciably inhibited when anti- $A\beta$  antibodies or ligands specific for the C-terminal or central  $A\beta$  region are used.

Using atomistic peptide models in explicit solvent, in this study we elucidated key structural differences between three  $A\beta$ -42 peptides with distinct aggregation rates, namely, the wild-type (WT), a soluble (GM6), and a highly insoluble (Dutch) variant. Specifically, the markers that we used for structural characterization indicate that the monomers have dissimilar stability primarily at the N-terminal (RES. 1–10). This behavior contrasts with the one observed for the CHC and C-terminal regions, for which comparable dynamics and/or structural features are observed. Of interest, the relative N-terminal rigidity of these monomers is consistent with their relative aggregation tendency (though a direct correlation with the complex  $A\beta$  aggregation mechanisms is beyond the scope of our single-molecule study).

Our simulations show that the N-terminal region of the GM6 mutant forms a well-conserved  $\beta$ -hairpin motif that significantly stabilizes this segment relative to that of the WT and Dutch peptides. Furthermore, despite being largely devoid of secondary structure, the N-terminal of the WT monomer still displays restricted motion when compared to that of the Dutch mutant, possibly due to frequent contacts between its N- and C-terminal tails as well as recurrent interactions in the region encompassing RES. 3–18 (e.g., H-bonds between E3 and K16 or L17). These results are consistent with our N-terminal  $S^2$  parameter,  $\overline{\text{RMSF}}_{\text{back}}$ , and  $\text{SASA}_{\text{H}\phi}$  analyses. Our observations are also in line with those of former studies that used an analogous  $A\beta$  model,<sup>45,46</sup> regarding a decreased flexibility in the N-terminal region of the "more soluble" WT  $A\beta$ -40 variant, relative to that of WT  $A\beta$ -42. Those authors remark that the WT  $A\beta$ -40 monomer forms a small helical structure that stabilizes the N-terminal. Thus, the increased solubility of WT  $A\beta$ -40 over WT  $A\beta$ -42 and similarly that of GM6 over WT  $A\beta$ -40 may be primarily due to an increase in N-terminal stability promoted by a better conserved motif in this region.

Unlike the N-terminal, the CHC and C-terminal regions of the three monomers show no clear distinguishing traits among them. All peptides regularly display structured motifs at all or part of the CHC, and we found no appreciable changes in structure,  $S^2$  parameter,  $\overline{\text{RMSF}}_{\text{back}}$ , or  $\text{SASA}_{\text{H}\phi}$  among the CHC of  $A\beta$ -42 monomers with widely varying solubilities (e.g., Dutch and WT). Nevertheless, mutagenesis studies have previously identified this

region as a major modulator of  $\text{A}\beta$  aggregation rate,<sup>78</sup> possibly due to cooperative interactions between RES. 17–21 and the remainder of the peptide (see Figure 7), or with various segments of other  $\text{A}\beta$ -42 monomers upon oligomerization, rather than being solely a local effect. Moreover, the CHC is contained within the fibril-forming core and may be responsible for the  $\alpha-\beta$  transition observed during aggregation/fibrillization.<sup>17</sup> Thus, it is also likely that this region plays an important role in the  $\text{A}\beta$ 's oligomerization pathways.

The C-terminal region of WT  $\text{A}\beta$ -42 has been found to possess less flexibility than that of WT  $\text{A}\beta$ -40,<sup>16,73,79,80</sup> a disparity that has led to the conjecture that  $\text{A}\beta$  monomer aggregation may be seeded in the C-terminal and facilitated by the formation of stabilizing  $\beta$ -sheets in the 42-residue peptide,<sup>39,46</sup> which lower the entropic cost for aggregation. Our results indicate that the insoluble  $\text{A}\beta$ -42 variants, unlike the GM6 monomer, have propensity toward the formation of  $\beta$ -hairpin motifs (see Figures 5a and 5b) in their C-terminal. However, we found no statistically significant difference in the C-terminal SASA<sub>H $\phi$</sub>  between the three monomers, as well as analogous C-terminal S<sup>2</sup> parameter and RMSF<sub>back</sub> values between the Dutch and GM6 mutants, suggesting comparable flexibility and hydrophobicity between the monomers of variants displaying markedly different aggregation rates. These later observations appear inconsistent with the behavior that would be expected for a simplistic C-terminal hydrophobic tail aggregation mechanism. However, given that this work is limited to the study of the isolated  $\text{A}\beta$ -42 monomers in water, it is still plausible that C-terminal aggregation may be favored by specific conformational changes upon dimerization or alterations to the environment's conditions (e.g.,  $\text{A}\beta$  concentration or pH).

Overall, this work takes a step forward toward the identification of structural traits of  $\text{A}\beta$  monomers that may have relevance to the  $\text{A}\beta$ -42 oligomerization mechanisms. Our findings are consistent with the effectiveness displayed by anti- $\text{A}\beta$  antibodies specific for this peptide's N-terminal (RES. 1–10) epitope<sup>81</sup> in reducing cerebral  $\text{A}\beta$  deposition in clinical trials. Specifically, our results allow us to hypothesize that oligomerization may be inhibited when the N-terminal region of  $\text{A}\beta$  is stabilized upon binding of N-terminal specific anti- $\text{A}\beta$  antibodies and ligands, directly at the monomer level. The latter argument is consistent with conventional energetic premises suggesting that more *native-like* structures with increased stability and a lower exposed hydrophobic surface (e.g., GM6) would have reduced probability of association and encounter higher energetic barriers when undergoing any conformational change taking place during the early stages of oligomerization. Moreover, various studies on short peptides suggest a close relation between basic physicochemical properties such as the ones analyzed in this work and the peptides' aggregation propensities.<sup>82–84</sup>

Conversely, the conjecture that  $\text{A}\beta$  monomer N-terminal stabilization could lead to reduced oligomerization does not necessarily imply that the N-terminal will be a seed for  $\text{A}\beta$  aggregation if this region is unstable. In fact, experimental studies undermine this possibility, by reporting that: (i) the N-terminal region is not part of the fibril forming core<sup>75</sup> and is still accessible for N-terminal specific anti- $\text{A}\beta$  therapy within a fibrillar arrangement<sup>68</sup> and (ii) anti- $\text{A}\beta$  antibodies also recognize  $\text{A}\beta$ 's N-terminal binding region in oligomers,<sup>67</sup> suggesting an exposed N-terminal.

Despite being an improbable oligomerization site, the N-terminal could act as a "catalyst" of aggregation when it is unstable.

Furthermore, we anticipate that the stabilization of the N-terminal leads to the formation of strong contacts between this region and RES. 22–30 (e.g., D1–E22, E3–K28, F4–G29, D7–N27, and H6–N27 in the GM6 variant), replacing weaker bonds that allow structural changes that are favorable for oligomerization, at least at its early stages.

Increasing evidence suggests that the CHC, C, and N terminals play an important role in what appears to be a stepwise transition with multiple oligomerization pathways.<sup>3,4</sup> Given that these key regions interplay in the aggregation process, an accurate identification of plausible oligomerization mechanisms entails the exploration of a very complex multidimensional conformational space; this is true even for the simplest case (i.e., dimerization). Initial approximations such as rigid backbone docking calculations are useful only if the interacting structures are representative of the  $\text{A}\beta$  ensemble of interest. Moreover, for flexible peptides such as WT  $\text{A}\beta$ -42, binding may be optimized through conformational changes that make rigid body docking analyses inadequate. Thus, a sensible direction of future research on  $\text{A}\beta$  peptide dynamics likely involves an accurate determination of the structure (e.g., crystallization) of more soluble mutants, such as GM6, that can greatly assist in the validation/improvement of current in silico models, which in turn can be used to improve the structural prediction of the WT  $\text{A}\beta$  monomers used for further oligomerization analyses.

Ongoing efforts on this topic are focused on the study of the dynamics of homo-/heterodimers assembled from central structures of the three variants analyzed in this work.

## ASSOCIATED CONTENT

**S Supporting Information.** A preliminary analysis leading to the identification of the representative time periods for the  $\text{A}\beta$ -42 variants studied. This material is available free of charge via the Internet at <http://pubs.acs.org>.

## AUTHOR INFORMATION

### Corresponding Author

\*E-mail: fe13@cornell.edu

## ACKNOWLEDGMENT

The authors are grateful for support from the National Science Foundation, Award No. CBET 0933092, and acknowledge Corning Inc. for kindly providing computational resources that allowed the completion of this work.

## REFERENCES

- (1) Haass, C.; Selkoe, D. J. *Nat. Rev. Mol. Cell Biol.* **2007**, 8, 101–112.
- (2) Shankar, G. M.; Li, S.; Mehta, T. H.; Garcia-Munoz, A.; Shepardson, N. E.; Smith, I.; Brett, F. M.; Farrell, M. A.; Rowan, M. J.; Lemere, C. A.; Regan, C. M.; Walsh, D. M.; Sabatini, B. L.; Selkoe, D. J. *Nat. Med.* **2008**, 14, 837–842.
- (3) Bernstein, S. L.; Dupuis, N. F.; Lazo, N. D.; Wyttenbach, T.; Condron, M. M.; Bitan, G.; Teplow, D. B.; Shea, J.; Ruotolo, B. T.; Robinson, C. V.; Bowers, M. T. *Nature Chem.* **2009**, 1, 326–331.
- (4) Bitan, G. *Proc. Natl. Acad. Sci.* **2002**, 100, 330–335.
- (5) Kayed, R.; Head, E.; Thompson, J. L.; McIntire, T. M.; Milton, S. C.; Cotman, C. W.; Glabe, C. G. *Science* **2003**, 300, 486–489.
- (6) Walsh, D. M.; Tseng, B. P.; Rydel, R. E.; Podlisny, M. B.; Selkoe, D. J. *Biochemistry* **2000**, 39, 10831–10839.

- (7) Ward, R. V.; Jennings, K. H.; Jepras, R.; Neville, W.; Owen, D. E.; Hawkins, J.; Christie, G.; Davis, J. B.; George, A.; Karra, E. H.; Howlett, D. R. *Biochem. J.* **2000**, *348*, 137–144.
- (8) Ono, K.; Condron, M. M.; Teplow, D. B. *J. Biol. Chem.* **2010**, *285*, 23186–23197.
- (9) Zhang, S. *J. Struct. Biol.* **2000**, *130*, 130–141.
- (10) Hou, L.; Shao, H.; Zhang, Y.; Li, H.; Menon, N. K.; Neuhaus, E. B.; Brewer, J. M.; Byeon, I. L.; Ray, D. G.; Vitek, M. P.; Iwashita, T.; Makula, R. A.; Przybyla, A. B.; Zagorski, M. G. *J. Am. Chem. Soc.* **2004**, *126*, 1992–2005.
- (11) Melquiond, A.; Dong, X.; Mousseau, N.; Derreumaux, P. *Curr. Alzheimer Res.* **2008**, *5*, 244–250.
- (12) Wood, S. J.; Wetzel, R.; Martin, J. D.; Hurle, M. R. *Biochemistry* **1995**, *34*, 724–730.
- (13) Kirkadze, M. D.; Condron, M. M.; Teplow, D. B. *J. Mol. Biol.* **2001**, *312*, 1103–1119.
- (14) Lazo, N. D.; Grant, M. A.; Condron, M. C.; Rigby, A. C.; Teplow, D. B. *Protein Sci.* **2005**, *14*, 1581–1596.
- (15) Tomaselli, S.; Esposito, V.; Vangone, P.; van Nuland, N. A. J.; Bonvin, A. M. J. J.; Guerrini, R.; Tancredi, T.; Temussi, P. A.; Picone, D. *ChemBioChem* **2006**, *7*, 257–267.
- (16) Lim, K. H.; Henderson, G. L.; Jha, A.; Louhivuori, M. *Chem-BioChem* **2007**, *8*, 1251–1254.
- (17) Szabo, Z.; Klement, K.; Jost, K.; Zarandi, M.; Soos, K.; Penke, B. *Biochem. Biophys. Res. Commun.* **1999**, *265*, 297–300.
- (18) Sticht, H.; Bayer, P.; Willbold, D.; Dames, S.; Hilbich, C.; Beyreuther, K.; Frank, R. W.; Rösch, P. *Eur. J. Biochem.* **1995**, *233*, 293–298.
- (19) Crescenzi, O.; Tomaselli, S.; Guerrini, R.; Salvadori, S.; D'Ursi, A. M.; Temussi, P. A.; Picone, D. *Eur. J. Biochem.* **2002**, *269*, 5642–5648.
- (20) Chen, W.; Mousseau, N.; Derreumaux, P. *J. Chem. Phys.* **2006**, *125*, 084911–8.
- (21) Khandogin, J.; Brooks, C. L. *Proc. Natl. Acad. Sci. U.S.A.* **2007**, *104*, 16880–16885.
- (22) Chebaro, Y.; Mousseau, N.; Derreumaux, P. *J. Phys. Chem. B* **2009**, *113*, 7668–7675.
- (23) Cecchini, M.; Curcio, R.; Pappalardo, M.; Melki, R.; Caflisch, A. *J. Mol. Biol.* **2006**, *357*, 1306–1321.
- (24) Jang, S.; Shin, S. *J. Phys. Chem. B* **2008**, *112*, 3479–3484.
- (25) Anand, P.; Nandel, F. S.; Hansmann, U. H. E. *J. Chem. Phys.* **2008**, *129*, 195102.
- (26) Cecchini, M.; Rao, F.; Seeber, M.; Caflisch, A. *J. Chem. Phys.* **2004**, *121*, 10748.
- (27) Krone, M. G.; Baumketner, A.; Bernstein, S. L.; Wyttenbach, T.; Lazo, N. D.; Teplow, D. B.; Bowers, M. T.; Shea, J. *J. Mol. Biol.* **2008**, *381*, 221–228.
- (28) Baumketner, A.; Krone, M. G.; Shea, J. *Proc. Natl. Acad. Sci.* **2008**, *105*, 6027–6032.
- (29) Wei, G.; Shea, J. *Biophys. J.* **2006**, *91*, 1638–1647.
- (30) Baumketner, A.; Bernstein, S. L.; Wyttenbach, T.; Lazo, N. D.; Teplow, D. B.; Bowers, M. T.; Shea, J. *Protein Sci.* **2006**, *15*, 1239–1247.
- (31) Baumketner, A.; Shea, J. *J. Mol. Biol.* **2007**, *366*, 275–285.
- (32) Daidone, I.; Simona, F.; Roccatano, D.; Broglia, R. A.; Tiana, G.; Colombo, G.; Di Nola, A. *Proteins* **2004**, *57*, 198–204.
- (33) Nguyen, P. H.; Li, M. S.; Stock, G.; Straub, J. E.; Thirumalai, D. *Proc. Natl. Acad. Sci.* **2007**, *104*, 111–116.
- (34) Huet, A.; Derreumaux, P. *Biophys. J.* **2006**, *91*, 3829–3840.
- (35) Han, W.; Wu, Y. *Proteins* **2007**, *66*, 575–587.
- (36) Kassler, K.; Horn, A. H. C.; Sticht, H. *J. Mol. Model.* **2009**, *16*, 1011–1020.
- (37) Kittner, M.; Knecht, V. *J. Phys. Chem. B* **2010**, *114*, 15288–15295.
- (38) Wu, C.; Murray, M. M.; Bernstein, S. L.; Condron, M. M.; Bitan, G.; Shea, J.; Bowers, M. T. *J. Mol. Biol.* **2009**, *387*, 492–501.
- (39) Yang, M.; Teplow, D. *J. Mol. Biol.* **2008**, *384*, 450–464.
- (40) Mitternacht, S.; Staneva, I.; Härd, T.; Irbäck, A. *Proteins* **2010**, *78*, 2600–2608.
- (41) Kim, S.; Takeda, T.; Klimov, D. K. *Biophys. J.* **2010**, *99*, 1949–1958.
- (42) Vitalis, A.; Caflisch, A. *J. Mol. Biol.* **2010**, *403*, 148–165.
- (43) Urbanc, B.; Betnel, M.; Cruz, L.; Bitan, G.; Teplow, D. B. *J. Am. Chem. Soc.* **2010**, *132*, 4266–4280.
- (44) Baumketner, A.; Bernstein, S. L.; Wyttenbach, T.; Bitan, G.; Teplow, D. B.; Bowers, M. T.; Shea, J. *Protein Sci.* **2006**, *15*, 420–428.
- (45) Sgourakis, N. G.; Merced-Serrano, M.; Boutsidis, C.; Drineas, P.; Du, Z.; Wang, C.; Garcia, A. E. *J. Mol. Biol.* **2011**, *405*, 570–583.
- (46) Sgourakis, N. G.; Yan, Y.; McCallum, S. A.; Wang, C.; Garcia, A. E. *J. Mol. Biol.* **2007**, *368*, 1448–1457.
- (47) Luttmann, E.; Fels, G. *Chem. Phys.* **2006**, *323*, 138–147.
- (48) Flöck, D.; Colacino, S.; Colombo, G.; Di Nola, A. *Proteins* **2006**, *62*, 183–192.
- (49) Triguero, L.; Singh, R.; Prabhakar, R. *J. Phys. Chem. B* **2008**, *112*, 2159–2167.
- (50) Kaminski, G. A.; Friesner, R. A.; Tirado-Rives, J.; Jorgensen, W. L. *J. Phys. Chem. B* **2001**, *105*, 6474–6487.
- (51) Jorgensen, W. L.; Chandrasekhar, J.; Madura, J. D.; Impey, R. W.; Klein, M. L. *J. Chem. Phys.* **1983**, *79*, 926–935.
- (52) Petkova, A. T. *Proc. Natl. Acad. Sci.* **2002**, *99*, 16742–16747.
- (53) Sugita, Y.; Okamoto, Y. *Chem. Phys. Lett.* **1999**, *314*, 141–151.
- (54) Brenner, P.; Sweet, C. R.; VonHandorf, D.; Izaguirre, J. A. *J. Chem. Phys.* **2007**, *126*, 074103.
- (55) Wurth, C.; Guimard, N. K.; Hecht, M. H. *J. Mol. Biol.* **2002**, *319*, 1279–1290.
- (56) Kim, W.; Hecht, M. H. *Proc. Natl. Acad. Sci.* **2006**, *103*, 15824–15829.
- (57) Fisher, A. C.; Kim, W.; Delisa, M. P. *Protein Sci.* **2006**, *15*, 449–458.
- (58) Murakami, K.; Irie, K.; Morimoto, A.; Ohigashi, H.; Shindo, M.; Nagao, M.; Shimizu, T.; Shirasawa, T. *J. Biol. Chem.* **2003**, *278*, 46179–46187.
- (59) Pérez, A.; Morelli, L.; Cresto, J. C.; Castaño, E. M. *Neurochem. Res.* **2000**, *25*, 247–255.
- (60) Davis, J.; Van Nostrand, W. E. *Proc. Natl. Acad. Sci. U.S.A.* **1996**, *93*, 2996–3000.
- (61) Fraser, P. E.; Nguyen, J. T.; Inouye, H.; Surewicz, W. K.; Selkoe, D. J.; Podlisny, M. B.; Kirschner, D. A. *Biochemistry* **1992**, *31*, 10716–10723.
- (62) Waal, R. M. W. D.; Schipper, J. J.; Nostrand, W. E. V. *J. Neurochem.* **1997**, *68*, 1135–1141.
- (63) Irie, K.; Murakami, K.; Masuda, Y.; Morimoto, A.; Ohigashi, H.; Ohashi, R.; Takegoshi, K.; Nagao, M.; Shimizu, T.; Shirasawa, T. *J. Biosci. Bioeng.* **2005**, *99*, 437–447.
- (64) Massi, F.; Straub, J. E. *Biophys. J.* **2001**, *81*, 697–709.
- (65) Cruz, L.; Urbanc, B.; Borreguero, J. M.; Lazo, N. D.; Teplow, D. B.; Stanley, H. E. *Proc. Natl. Acad. Sci. U.S.A.* **2005**, *102*, 18258–18263.
- (66) Spoel, D. V. D.; Lindahl, E.; Hess, B.; Groenhof, G.; Mark, A. E.; Berendsen, H. J. C. *J. Comput. Chem.* **2005**, *26*, 1701–1718.
- (67) Velez-Vega, C.; Fenwick, M. K.; Escobedo, F. A. *J. Phys. Chem. B* **2009**, *113*, 1785–1795.
- (68) Nosé, S. *J. Chem. Phys.* **1984**, *81*, 511.
- (69) Hoover, W. *Phys. Rev. A* **1985**, *31*, 1695–1697.
- (70) Hess, B.; Bekker, H.; Berendsen, H. J. C.; Fraaije, J. G. E. M. *J. Comput. Chem.* **1997**, *18*, 1463–1472.
- (71) Kabsch, W.; Sander, C. *Biopolymers* **1983**, *22*, 2577–2637.
- (72) Humphrey, W.; Dalke, A.; Schulten, K. *J. Mol. Graphics* **1996**, *14*, 33–38.
- (73) Riek, R.; Guntert, P.; Dobeli, H.; Wipf, B.; Wuthrich, K. *Eur. J. Biochem.* **2001**, *268*, 5930–5936.
- (74) Dobson, C. M. *Trends Biochem. Sci.* **1999**, *24*, 329–332.
- (75) Luhrs, T. *Proc. Natl. Acad. Sci.* **2005**, *102*, 17342–17347.
- (76) Orner, B. P.; Liu, L.; Murphy, R. M.; Kiessling, L. L. *J. Am. Chem. Soc.* **2006**, *128*, 11882–11889.
- (77) Lee, M.; Bard, F.; Johnson-Wood, K.; Lee, C.; Hu, K.; Griffith, S. G.; Black, R. S.; Schenk, D.; Seubert, P. *Ann. Neurol.* **2005**, *58*, 430–435.

- (78) de Groot, N. S.; Aviles, F. X.; Vendrell, J.; Ventura, S. *FEBS J.* **2006**, *273*, 658–668.
- (79) Yan, Y.; Wang, C. *J. Mol. Biol.* **2006**, *364*, 853–862.
- (80) Yan, Y.; Liu, J.; Mccallum, S.; Yang, D.; Wang, C. *Biochem. Biophys. Res. Commun.* **2007**, *362*, 410–414.
- (81) Szabo, P.; Relkin, N.; Weksler, M. *Autoimmun. Rev.* **2008**, *7*, 415–420.
- (82) Lin, E. I.; Shell, M. S. *J. Phys. Chem. B* **2010**, *114*, 11899–11908.
- (83) Tartaglia, G. G.; Cavalli, A.; Pellarin, R.; Caflisch, A. *Protein Sci.* **2004**, *13*, 1939–1941.
- (84) Chiti, F.; Stefani, M.; Taddei, N.; Ramponi, G.; Dobson, C. M. *Nature* **2003**, *424*, 805–808.